# Iodide Manipulation Using Zinc Additives for Efficient Perovskite Solar Minimodules

**Jinsong Huang** ( jhuang@unc.edu )
University of North Carolina at Chapel Hill https://orcid.org/0000-0002-0509-8778
**Md Aslam Uddin**
University of North Carolina at Chapel Hill https://orcid.org/0000-0002-9780-2864
**Prem Jyoti Singh Rana**
University of North Carolina at Chapel Hill
**Zhenyi Ni**
University of North Carolina at Chapel Hill
**Guang Yang**
UNC https://orcid.org/0000-0003-0994-9178
**Mingze Li**
University of North Carolina at Chapel Hill
**Mengru Wang**
University of North Carolina Chapel Hill https://orcid.org/0000-0003-1864-2207
**Hangyu Gu**
University of North Carolina at Chapel Hill https://orcid.org/0000-0003-0378-9185
**Hengkai Zhang**
University of North Carolina at Chapel Hill
**Benjia Dak Dou**
CubicPV Inc.

**Article**

**Keywords:**

**Posted Date:** April 20th, 2023

**DOI:** https://doi.org/10.21203/rs.3.rs-2769547/v1



**Additional Declarations: Yes** there is potential Competing Interest. The authors declare the following competing financial interest: Benjia Dak Dou is employed by CubicPV Inc., a manufacturer of solar

photovoltaic equipment and materials.

**Version of Record:** A version of this preprint was published at Nature Communications on February 14th, 2024. See the published version at https://doi.org/10.1038/s41467-024-45649-6.

# Iodide Manipulation Using Zinc Additives for Efficient Perovskite Solar Minimodules

Md Aslam Uddin,[1] Prem Jyoti Singh Rana,[1] Zhenyi Ni,[1] Guang Yang,[1] Mingze Li,[1] Mengru Wang,[1] Hangyu Gu,[1] Hengkai Zhang,[1] Benjia Dak Dou,[2] and Jinsong Huang*[1,3]

[1]Department of Applied Physical Sciences, University of North Carolina at Chapel Hill, Chapel Hill, NC 27599, USA

[2]CubicPV Inc., Bedford, MA 01730, USA

[3]Department of Chemistry, University of North Carolina at Chapel Hill, Chapel Hill, NC 27599, USA

*Corresponding author's e-mail: jhuang@unc.edu

## Abstract

Interstitial iodides are the most important type of defects in perovskite solar cells that limits efficiency and stability. They can be generated during solution, film, and device processing and further accelerate device degradation. Herein, we find that introducing a small amount of an organozinc compound- zinc trifluoromethanesulfinate ($Zn(OOSCF_3)_2$) in the perovskite solution can control the iodide defects in resultant perovskites ink and films. $CF_3SOO^-$ vigorously suppresses molecular iodine formation in the perovskites by reducing it to iodide, while zinc cations can precipitate out excess iodide by forming a Zn-Amine complex so that the iodide interstitials in the resultant perovskite films can be suppressed. The perovskite films using these additives show improved photoluminescence quantum efficiency and reduce deep trap density, despite that zinc cations reduce the perovskite grain size and iodide interstitials. The zinc

additives facilitate the formation of more uniform perovskite films on large-area substrates (78-108 $cm^2$) in the blade-coating process. Fabricated minimodules show power conversion efficiencies of 19.60% and 19.21% with aperture areas of 84 and 108 $cm^2$, respectively, as certified by National Renewable Energy Laboratory (NREL), the highest efficiency certified for minimodules of these sizes.

## Introduction

Despite the efficiency of small perovskite solar cells already reaching over 25.7%, the perovskite module efficiency is still far behind that of silicon modules.[1,2] To realize high efficiency modules, it is important to use scalable methods to fabricate efficient solar cells, and the resultant cell-to-module efficiency loss needs to be small. Minimizing the cell-to-minimodule efficiency loss needs to produce not only uniform perovskite films over a large area in ambient conditions but also it needs good passivation uniformity and good uniformity of charge transport materials. Nonuniformity of the photoactive layers mainly impacts module short circuit current density ($J_{SC}$) and fill factor ($FF$), despite the loss of averaged open circuit voltage ($V_{OC}$) of subcells from modules is sometimes observed.

Several efforts reported promising improvements of minimodules with small aperture areas by improving perovskite phase stability,[3,4] hole transporting layer (HTL)/perovskite and perovskite/electron transporting layer (ETL) interfaces and their contact,[5–7] and charge transport properties.[6–8] Even after all these efforts, relative cell-to-module efficiency loss is *ca.* 15-20% with an aperture area between 20-50 $cm^2$.[5–9] None of these studies addresses other important issues, such as iodide interstitial defects to reduce the cell-to-module efficiency loss. Nonuniformity arises from oxidized perovskite inks, especially oxidation of iodide to molecular

iodine when inks are exposed to ambient environment during the fabrication process in the ambient conditions. In addition, introduction of 2D-iodide salts such as phenethylammonium iodide (PEAI) and dodecyl ammonium iodide (DDAI) in the perovskite inks increases more iodide and thus introduce more iodide interstitials. Both molecular iodine generation in inks and many iodide interstitials in the perovskite films introduce nonuniformity in perovskite films and thus lead to larger cell-to-module efficiency loss apart from the dead area and ITO resistive losses in minimodule design and fabrication.[10]

In our study, we address these two issues by introducing organozinc salts in the perovskite inks. In the organozinc compound, organic anions ($CF_3SOO^-$ ions) vigorously reduce the molecular iodine into iodides, whereas zinc cations can take away excess iodide by forming a Zn-Amine complex in the perovskite inks. Therefore, we are able to demonstrate large aperture area modules (78-108 $cm^2$) with high reproducibility by improving the perovskite film quality and uniformity. Minimodules with an aperture area of 78-108 $cm^2$ show an average aperture area efficiency between 19.21% and 19.55%, with NREL certified efficiency of 19.60% at a much larger aperture area of 79.67 $cm^2$.

**Results and Discussion:**

**Organozinc additive and Device Performance**

Metal salts and their complexes have been frequently used to tune the composition or modify the surface of perovskites to enhance the solar cell performance, especially $V_{OC}$ and $FF$.[11–15] Previously, zinc halide salts ($ZnX_2$, X = Cl, Br, or I) were reported to improve the small device performance.[13] Here we modified the organozinc additives with different organic an ions including $–COO^–$, $–SOO^–$, and $–SO_2O^–$ anions having the strong affinity to the $Pb^{2+}$ ion.[16] We

thus added different organozinc salts, including zinc formate [$Zn(OOCH)_2$], zinc acetate [$Zn(OOCCH_3)_2$], zinc trifluoroacetate [$Zn(OOCCF_3)_2$], zinc trifluoromethane sulfinate [$Zn(OOSCF_3)_2$], and zinc trifluoromethane sulfonate [$Zn(OO_2SCF_3)_2$] as listed in **Fig.1a** into the perovskite ink and evaluated their impacts on the device performances. To verify the effects of organozinc compounds, we first fabricated small area devices with a mixed cation composition of methylammonium (30%)-formamidinium (70%) lead iodide ($FA_{0.3}MA_{0.7}PbI_3$) as an active layer with varying the concentration of each organozinc additive by following our established blading procedure.[17,18]

**Fig.1b** summarizes the performance statistics of the devices with optimized concentration (**Fig. S1** for other concentrations) of different organozinc additives. The control devices deliver an average efficiency of 22.22±0.69%, agreeing with previous study.[5,17] Devices with organozinc additives of $Zn(OOCH)_2$, $Zn(OOCCH_3)_2$, $Zn(OOCCF_3)_2$, $Zn(OOSCF_3)_2$, and $Zn(OO_2SCF_3)_2$ deliver the average efficiency of 22.59±0.44%, 22.03±0.48%, 22.28±0.86%, 23.61±0.30%, and 22.83±0.40% at specific molar concentrations (compared to the Pb-concentration) of 0.42%, 0.28%, 0.42%, 0.28%, and 0.42%, respectively. Among all the additives, $Zn(OOSCF_3)_2$ delivers the highest efficiency at almost all the additive concentrations. At the optimized concentration of 0.28% for $Zn(OOSCF_3)_2$, small devices are highly reproducible with all-around best device parameters as shown by the *J-V* characteristics from seven devices shown in **Fig.S2.** All the device performance parameters from 30 devices from different batches are summarized in **Table S1,** which again confirms the excellent reproducibility for these high-performance small area devices.

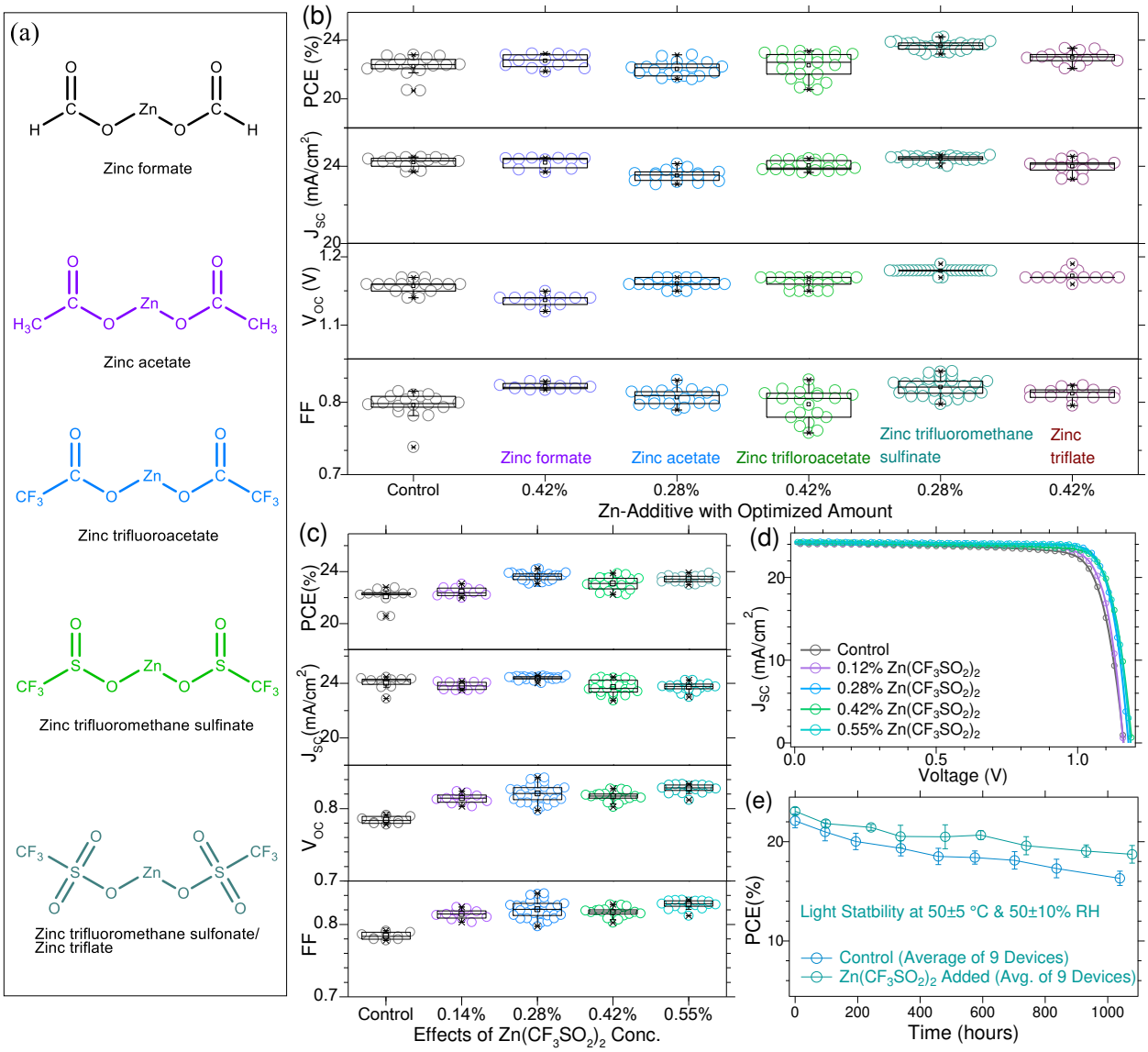


**Fig.1. Photovoltaic performance of small area cells. (a)** molecular structures of organozinc compounds as additives, **(b)** the performance statistics of the small devices with optimized concentration of different organozinc additives, **(c)** solar cell performance for small devices with varied $Zn(OOSCF_3)_2$ concentrations, **(d)** *J-V* curves small devices with varied $Zn(OOSCF_3)_2$ concentrations, and **(e)** time-dependent PCE of control and small devices with 0.42% $Zn(OOSCF_3)_2$ at $V_{OC}$ condition under 1 sun of LED light at 50±5 ℃ and 50±10% RH. There were 9 devices tested for each type of devices. The devices have an active area of 0.08 cm$^2$.

We studied the impact of $Zn(OOSCF_3)_2$ concentration on solar cell performance by analyzing how the photovoltaic parameters changes. **Fig.1c-d** shows performance statistics and *J-V* curves of the solar cells with $Zn(OOSCF_3)_2$ of different concentration. With increased $Zn(OOSCF_3)_2$ concentration, the average $V_{OC}$ increased from 1.16±0.01 V for the control devices to 1.18±0.00 V for the devices with 0.28% $Zn(OOSCF_3)_2$, and the average FF increased from 0.80±0.02 for the control device to 0.82±0.01 for the devices with 0.28% $Zn(OOSCF_3)_2$. There was no clear trend for the variation of $J_{SC}$ with increased $Zn(OOSCF_3)_2$ concentration, despite that the devices with optimal 0.28% $Zn(OOSCF_3)_2$ also improved slightly compared to the control devices. The results indicate that $Zn(OOSCF_3)_2$ improves the device efficiency through the defect passivation as both $V_{OC}$ and *FF* are significantly improved.[19–22]

We also tested the light-soaking stability of the small control devices and devices with $Zn(OOSCF_3)_2$ under 1 sun light at open circuit condition, following ISOS-L-1. The devices were encapsulated using epoxy and tested in air with 50±20% relative humidity, where the LED solar simulator light heated up the devices to 55±5 ºC. The evolution of the efficiency with statistics is shown in **Fig.1e and S3**. The devices with $Zn(OOSCF_3)_2$ retained 81.2% of its initial efficiency after light soaking for 1078 hours, while the control devices retain 72.8% of their initial efficiency after 1039 hours of light soaking, showing that organozinc additives improved the light stability of perovskite solar cells.

After verifying the small device performance with the optimized concentration of $Zn(OOSCF_3)_2$, we blade coated large area (>78 cm2) perovskite films and fand fabricated minimodules with an aperture area of 78-108 $cm^2$ . The resultant perovskite films appear smooth and uniform (**Fig.2a and S4**). Minimodules have the same structure and fabrication procedures

as previously reported,[17,18] and a photograph of several fabricated minimodules is shown in **Fig.2b**. *J-V* characteristic curves of the minimodules with different aperture area are shown in **Fig.2c**. Minimodules with aperture area of 78 $cm^2$, 84 $cm^2$ and 108 $cm^2$ delivered champion efficiencies of 20.18% ($V_{OC}$ = 1.17 V; $J_{SC}$ = 21.45 $mA \cdot cm^{-2}$; and $FF$ = 0.801), 20.18% ($V_{OC}$ = 1.18 V; $J_{SC}$ = 21.99 $mA \cdot cm^{-2}$; $FF$ = 0.796), and 20.23% ($V_{OC}$ = 1.19 V; $J_{SC}$ = 22.04 $mA \cdot cm^{-2}$; and $FF$ = 0.772), respectively. It is also found that all the minimodules fabricated with 0.14-0.28% $Zn(OOSCF_3)_2$ showed very reproducible performance among 67 fabricated minimodules. Average efficiencies of minimodules with aperture areas of 78, 84, and 108 $cm^2$ are 19.47±0.50%, 19.55±0.47%, and 19.21±0.51%, respectively, as shown in **Fig.2d**. The detailed photovoltaic parameters of all the minimodules with different aperture area are summarized in **Table S2**. Similar minimodule performance regardless of the aperture area variation indicates uniform and high-quality perovskite films facilitated by the introduction of $Zn(OOSCF_3)_2$-organozinc compound. To verify their efficiency, we sent several minimodules to NREL for certification, and it showed a stabilized efficiency of 19.60% with an aperture area of ~80 $cm^2$, as shown in **Fig.2e**.

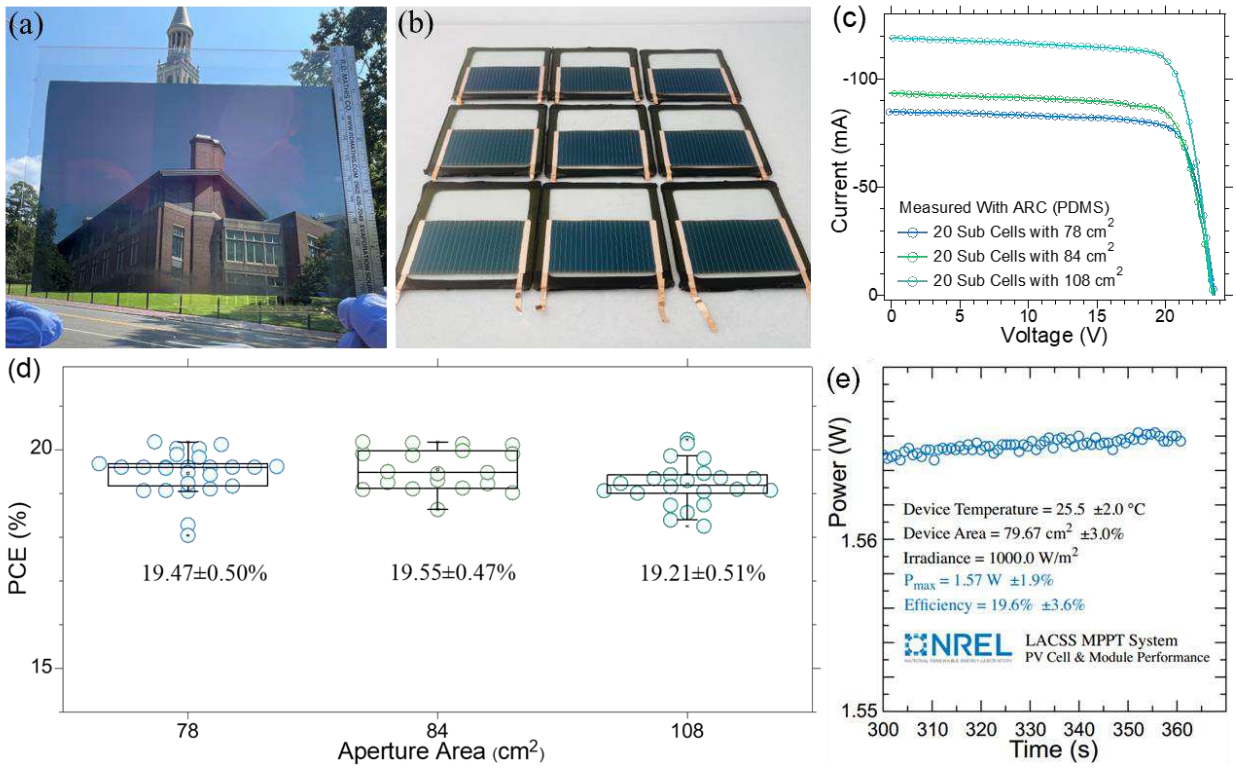


**Fig.2. Perovskite minimodule performance.** **(a)** a photograph of a bladed $FA_{0.3}MA_{0.7}PbI_3$ perovskite film on a ITO substrate with an area of ~130 $cm^2$, **(b)** a photograph of encapsulated minimodules with aperture areas of ~78 $cm^2$, **(c)** J-V curves of the minimodule with aperture areas of 78, 84, and 108 $cm^2$, respectively; **(d)** performance statistics of the minimodules with an aperture areas of 78, 84, and 108 $cm^2$, respectively; and **(e)** the stabilized power output of the champion minimodules fixed at a bias of maximum power point for 360 s tested by NREL.

This demonstration of larger area minimodules (80-110 $cm^2$) with a stabilized aperture efficiency of 19.60% (active area efficiency of 20.66%) and champion efficiency of 20.20% (active area efficiency of 21.24%), which is the record stabilized efficiency on ~100 $cm^2$ larger aperture area as summarized in the following **Table S3**.

**Optoelectronic and morphologic property change by $Zn(OOSCF_3)_2$**

To understand how $Zn(OOSCF_3)_2$ enhances the perovskite solar cell efficiency, we investigated the quality of $FA_{0.3}MA_{0.7}PbI_3$ perovskite thin films bladed on ITO/PTAA and carried out the optical and morphological characterization as shown in **Fig.3**. As shown in **Fig.3a**, among all the Zn additives, $Zn(OOSCF_3)_2$ improves the photoluminescence the most: it showed *ca.* 1.6 folds higher stead-state photoluminescence (PL) intensity than that of the control samples, indicating that Zn-additives reduce non-radiative recombination processes. PL quantum yield ($\Phi_{PL}$) and PL lifetime measurements were conducted on the control and the perovskite films with $Zn(OOSCF_3)_2$ with a structure of ITO/PTAA/Perovskite, and $\Phi_{PL}$ of the film with $Zn(OOSCF_3)_2$ is 1.4 folds of the control film (0.46% *vs.* 0.66%). $FA_{0.3}MA_{0.7}PbI_3$ films with $Zn(OOSCF_3)_2$ also showed ~6 nm blue shift of PL peak as shown in **Fig.3b**, indicating that $Zn(OOSCF_3)_2$ additives reduced the band-tail states.[23,24] The perovskite films with $Zn(OOSCF_3)_2$ also showed almost 3-times longer PL lifetime (0.7 μs for control film *vs* 2.0 μs for 0.28% $Zn(OOSCF_3)_2$ added film), as shown in **Fig.3c**. These studies conclude that $Zn(OOSCF_3)_2$ can passivate defects in the polycrystalline perovskites.

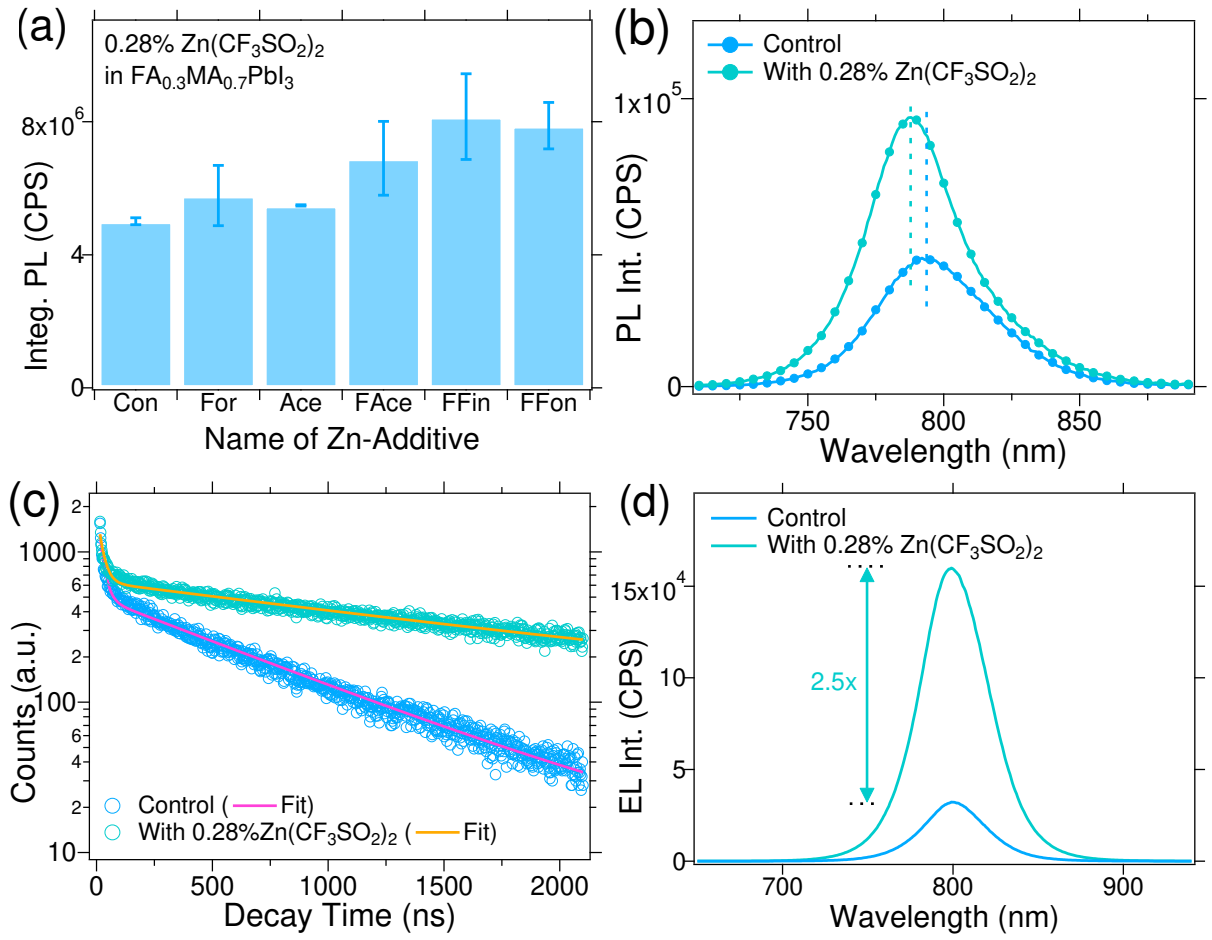


**Fig.3. Optical property of Perovskite Thin Films: (a)** integrated PL intensity of control and perovskite films with different types of Zn-additives, **(b)** PL intensity of perovskite films without and with $Zn(OOSCF_3)_2$, **(c)** PL decay curves of perovskite films with and without $Zn(OOSCF_3)_2$, and **(d)** electroluminescence (EL) spectra perovskite devices with and without $Zn(OOSCF_3)_2$.

We further collected electroluminescence (EL) spectra of the control device and the devices with $Zn(OOSCF_3)_2$ added in the perovskites at an injection current of 24 mA/cm$^2$ (close to the *Jsc* of device measured at 1 sun illumination). As shown in **Fig.3d**, EL intensity for the devices with $Zn(OOSCF_3)_2$ added films is *ca.* 2.5-folds higher than that of the control devices, indicating low non-radiative recombination losses that lead to the enhancement of $V_{OC}$.

Estimated $V_{OC}$ increase from the enhancement of EL intensity compared to the control device is found to be ~23.8 mV. Increase in *FF* can be explained by the change in the series resistance ($R_S$) and larger shunt resistance ($R_{Sh}$) of the devices. As shown in **Fig.S5** and **Table S4**, the champion devices with 0.28% $Zn(OOSCF_3)_2$ added perovskite films showed *ca.*1.4-fold higher $R_{Sh}$ and *ca.*1.1-fold lower $R_S$.

We also checked the morphology of $MA_{0.7}FA_{0.3}PbI_3$ perovskite films without/with $Zn(OOSCF_3)_2$ under scanning electron microscopy (SEM), to further find out whether $Zn(OOSCF_3)_2$ additive change grain growth behaviors. **Fig.4a, b** shows that the surface morphology of the perovskite films with $Zn(OOSCF_3)_2$ is much different than that of the control thin films. In addition, slightly smaller grain sizes were observed from the SEM cross-section images shown in **Fig.4c, d**, suggesting small metal ions such as $Zn^{2+}$ likely increase the nucleation rate during the crystallization. X-ray diffraction patten in **Fig.4e-f** shows that the crystallinity of the film with $Zn(OOSCF_3)_2$ is not changed. Generally, a smaller grain size would likely create more grain boundaries and thus induce more non-radiative charge recombination, which contrasts with the observed PL and EL enhancement, and device performance improvement. This indicates that the cations and anions have additional functions to passivate the introduced defects.

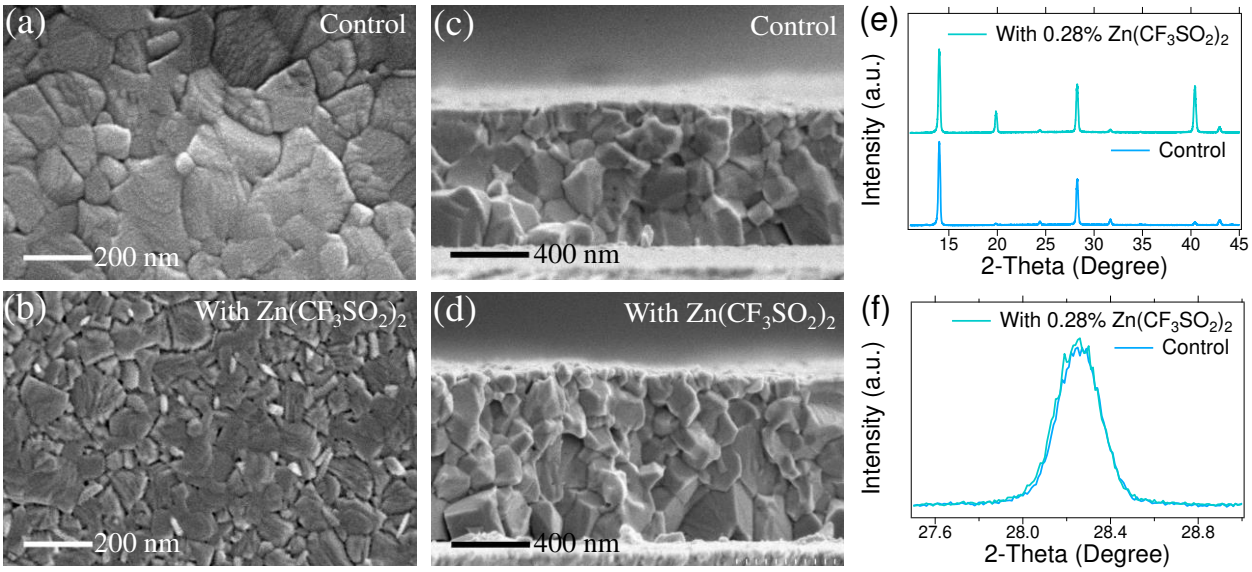


**Fig.4. Morphological Characterization of Perovskite Thin Films: (a-d)** comparison of top surface cross-section SEM images of control and $Zn(OOSCF_3)_2$ added perovskite films, **(e, d)** XRD patterns of control film and $Zn(OOSCF_3)_2$ added films showing the differences in peak intensity and broadness, respectively.

**Function of cations and anions of $Zn(OOSCF_3)_2$**

To verify if only $Zn^{2+}$ ions, or only organic anions, or both contribute device performance enhancement, we fabricated small devices with zinc halides as additive. As shown in **Fig.S6**, devices with $ZnCl_2$, $ZnBr_2$, and $ZnI_2$ showed comparable average efficiencies of 22.61±0.39%, 22.10±0.36%, and 22.45±0.40% after optimization, respectively. These efficiencies of the devices with $ZnX_2$ additives are comparable to that of the control devices, but much lower than that of the devices with $Zn(OOSCF_3)_2$ as an additive, indicating that the organic anions played the critical role in enhancing the device efficiency.

It is known that $CF_3SOO^-$ ions can generate $SO_2$ and $CF_3^-$ in presence of heat, acids, or bases,[25,] where $SO_2$ is a good reducing agent for the iodine and triiodide reduction.[25,26] Previous studies have shown that molecular iodine generation in perovskites under illumination is a common phenomenon and can accelerate the degradation of perovskites[17] We thus hypothesize that $CF_3SOO^-$ ions can reduce $I_2$ into $I_3^-$ in the perovskite solutions.[17] To verify it, we added $Zn(OOSCF_3)_2$ into the iodine solution with a molar ratio of 1:1, and observed that iodine color started to shifting from dark brown to transparent (**Fig.5a**). When the solution mixture of $I_2$ and $Zn(OOSCF_3)_2$ was put under the constant heat at 120 $^oC$ for over 15 minutes in presence of water or in a mixture MAI and FAI (7:3), iodine color disappears, as supported by the absorption spectra in **Fig.5b**. Therefore, the added $CF_3SOO^-$ ions can suppress $I_2$ formation in the perovskite solution, which is critical in the fabrication of perovskite solar cells in open air environment.

Since iodide interstitials form deep trapping states, and its concentration goes up with more iodide in precursor solution, we examined the iodide related deep trap density by the drive-level capacitance profiling (DLCP), and trap density of states (*tDOS*) by thermal admittance spectroscopy (TAS). The presence of $I_i^-$ in the perovskites in the devices can be readily identified by the TAS and DLCP measurements.[27] As shown in **Fig.5c**, the *tDOS* results reveals the trap density related to iodide interstitials actually slightly reduced in the $FA_{0.3}MA_{0.7}PbI_3$ polycrystalline thin film solar cells with the $Zn(OOSCF_3)_2$.[28] DCLP study reveals the deep trap density was reduced through the whole perovskite films as shown in **Fig.5d**. The reduction of the deep traps in the perovskite thin films explains the passivation effect and the resultant increase in $V_{OC}$.[28] However, it cannot be explained by $CF_3SOO^-$ ions, because $CF_3SOO^-$ ions cannot decrease the iodide interstitial concentration in the precursor concentration.

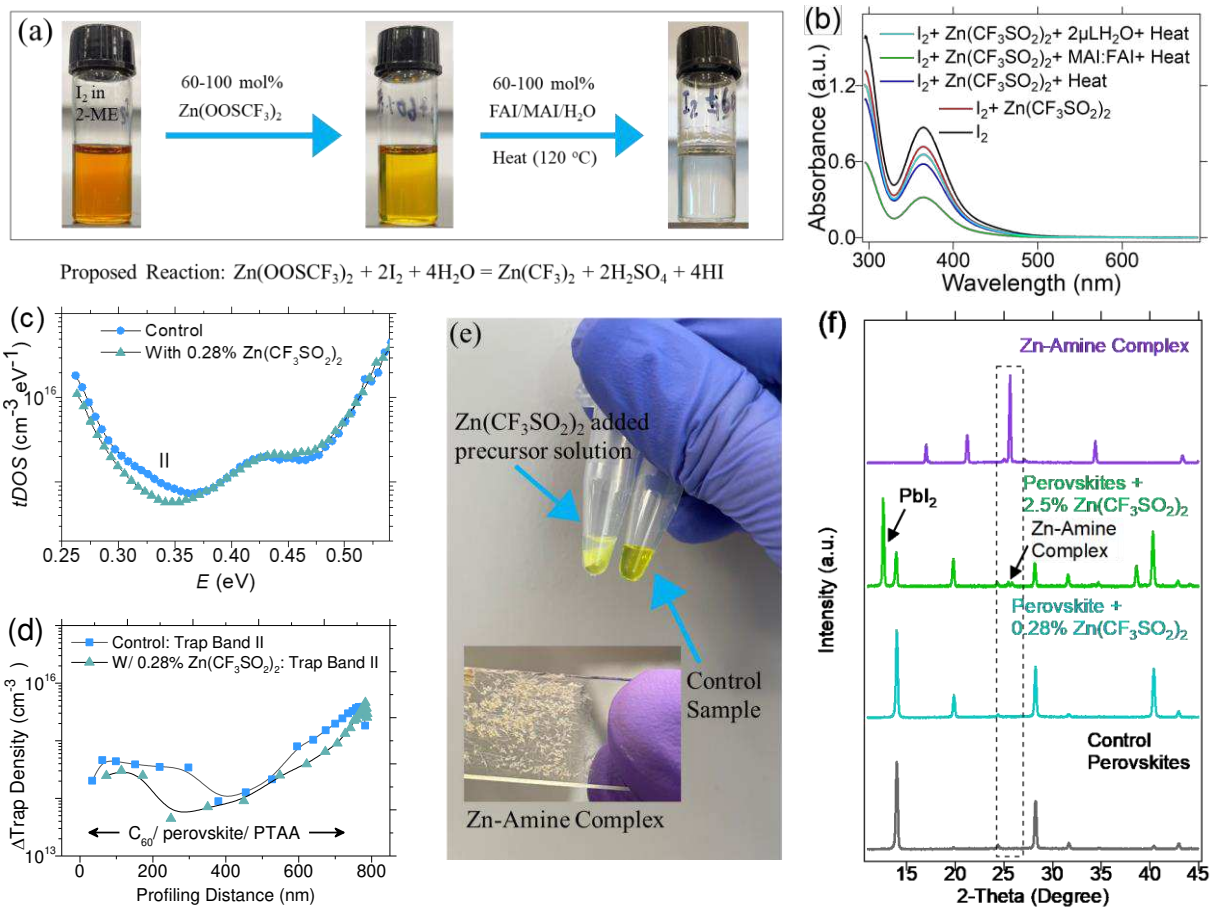


**Fig.5.** **(a)** optical images showing the roles of $CF_3SOO^-$ ions in the iodine reduction and the proposed reaction of the iodine reduction, **(b)** the absorption spectra collected at different conditions showing the iodine reduction of $CF_3SOO^-$ ions. In the experiment, 1.9 M $I_2$ solution in 2-ME, 60 mol% $Zn(OOSCF_3)_2$ in 2-ME w.r.t the $I_2$ solution, and 100 mol% a mixture of FAI and MAI (3:7) w.r.t the $I_2$ solution were used. For the absorption measurement, respective diluted solutions were used. **(c)** *tDOS* spectra of a $FA_{0.3}MA_{0.7}PbI_3$ polycrystalline thin film solar cells without and with $Zn(OOSCF_3)_2$. **(d)** spatial distributions of II with the trap depth of 0.35 eV in the $FA_{0.3}MA_{0.7}PbI_3$ solar cells without/with the addition of $Zn(OOSCF_3)_2$ under a forward bias of

+1.2 V measured by DLCP (note that $C_{60}$ or PTAA in the inset indicates the location that is close to the $C_{60}$ or PTAA layer of the device). **(e)** an optical photograph showing Zn-amine complex formation in the perovskite precursor solution when $Zn(OOSCF_3)_2$ is added in the perovskite precursor solution in an excess amount (e.g., 2.5 mol% to Pb). **(f)** XRD patterns of control film, films added with $Zn(OOSCF_3)_2$ at different molar concentration with respect to the $PbI_2$ concentration, and synthesized Zn-amine complex from a mixture of MAI, FAI, and $Zn(OOSCF_3)_2$.

We then examined the function of zinc cations. It is reported that $Zn^{2+}$ can form Zn-amine complex, $Zn(FA_xMA_{1-x})_4I_2$ [x has the maximum value of 1], in presence of primary amines or primary ammonium salts.[29–31] Zn-amine complex can easily be observed as it precipitates out for a while in the perovskite precursor solution when $Zn(OOSCF_3)_2$ was added in the perovskite precursor solution in an excess amount (e.g., 2.5 mol% to Pb). **Fig.5e** shows the difference between the control perovskite precursor and precursor added with 2.5 mol% $Zn(OOSCF_3)_2$, where the white precipitate is the Zn-amine complex. To verify if Zn-amine complex can be formed from MAI and FAI from a mixture of $FA_{0.3}MA_{0.7}I$, we synthesized this complex by mixing FAI, MAI, and $Zn(OOSCF_3)_2$ in 2-ME at room temperature. Formed complex (the inset image of **Fig.5e)** is rod-shaped and very crystalline as this complex is reported previously.[31] XRD pattern of this complex shown in **Fig.5f** gives very strong peak around 26º, which corresponds to the XRD peaks in the target perovskite films and further verifies the formation of Zn-amine complex.

We thus conclude that the reduction in trap density is caused by the $I^-$ precipitation by zinc salts. The formation of $Zn(FA_xMA_{1-x})_4I_2$ complex to takes excess $I^-$ ions from perovskite solution has important implications. In many perovskite solutions, iodide salts such as PEAI and

DDAI are introduced to form 2D perovskites for passivation, but they inevitably introduce more iodide and thus introduce more iodide interstitials. This provides an approach to modulate the iodide concentration in perovskite solution.

## Conclusion

In conclusion, we discovered a family of zinc additives which could improve the efficiency and stability of perovskite solar cells. Among all the zinc additives, $Zn(OOSCF_3)_2$ showed the best performance in passivating the defects of the perovskites despite its addition reduced grain sizes. The $CF_3SOO^-$ anions can reduce the generated iodine during perovskite solution or device aging, while the zinc cations can precipitate the excess iodide so that the iodide interstitial concentration reduced throughout the films, resulting in improved device efficiency and stability. These additives also improve the uniformity and reproducibility of perovskite films, which facilitated the demonstration of minimodules with larger aperture areas of 80-100 $cm^2$ with certified efficiency of 19.60%.

## Conflicts of Interest

The authors declare the following competing financial interest: Benjia Dak Dou is employed by CubicPV Inc., a manufacturer of solar photovoltaic equipment and materials.

## Acknowledgements

This material was mainly based upon work supported by the U.S. Department of Energy's Office of Energy Efficiency and Renewable Energy (EERE) under award DE-EE0009529 through CubicPV Inc. The module fabrication was based upon work supported by the U.S. Department of Energy's Office of Energy Efficiency and Renewable Energy (EERE) under the Solar Energy Technologies Office Award Number 38050. The views expressed in the article do not necessarily represent the views of the DOE or the U.S. Government.

**References:**

(1) Min, H.; Lee, D. Y.; Kim, J.; Kim, G.; Lee, K. S.; Kim, J.; Paik, M. J.; Kim, Y. K.; Kim, K. S.; Kim, M. G.; Shin, T. J.; Seok, S. Il. Perovskite Solar Cells with Atomically Coherent Interlayers on SnO2 Electrodes. *Nature* **2021**, *598* (7881), 444–450.

(2) Zhao, Y.; Ma, F.; Qu, Z.; Yu, S.; Shen, T.; Deng, H. X.; Chu, X.; Peng, X.; Yuan, Y.; Zhang, X.; You, J. Inactive (PbI2)2RbCl Stabilizes Perovskite Films for Efficient Solar Cells. *Science.* **2022**, *377* (6605), 531–534.

(3) Liu, X.; Chen, M.; Zhang, Y.; Xia, J.; Yin, J.; Li, M.; Brooks, K. G.; Hu, R.; Gao, X.; Kim, Y. H.; Züttel, A.; Luther, J. M.; Kinge, S.; Feng, Y.; Nazeeruddin, M. K. High-Efficiency Perovskite Photovoltaic Modules Achieved via Cesium Doping. *Chem. Eng. J.* **2022**, *431*, 133713.

(4) Bu, T.; Ono, L. K.; Li, J.; Su, J.; Tong, G.; Zhang, W.; Liu, Y.; Zhang, J.; Chang, J.; Kazaoui, S.; Huang, F.; Cheng, Y. B.; Qi, Y. Modulating Crystal Growth of Formamidinium–Caesium Perovskites for over 200 Cm2 Photovoltaic Sub-Modules. *Nat. Energy* **2022**, *7* (6), 528–536.

(5) Chen, S.; Dai, X.; Xu, S.; Jiao, H.; Zhao, L.; Huang, J. Stabilizing Perovskite-Substrate

Interfaces for High-Performance Perovskite Modules. *Science.* **2021**, *373* (6557), 902–907.

(6) Jeong, M.; Choi, I. W.; Yim, K.; Jeong, S.; Kim, M.; Choi, S. J.; Cho, Y.; An, J. H.; Kim, H. B.; Jo, Y.; Kang, S. H.; Bae, J. H.; Lee, C. W.; Kim, D. S.; Yang, C. Large-Area Perovskite Solar Cells Employing Spiro-Naph Hole Transport Material. *Nat. Photonics* **2022**, *16* (2), 119–125.

(7) Ding, Y.; Ding, B.; Kanda, H.; Usiobo, O. J.; Gallet, T.; Yang, Z.; Liu, Y.; Huang, H.; Sheng, J.; Liu, C.; Yang, Y.; Queloz, V. I. E.; Zhang, X.; Audinot, J. N.; Redinger, A.; Dang, W.; Mosconic, E.; Luo, W.; De Angelis, F.; Wang, M.; Dörflinger, P.; Armer, M.; Schmid, V.; Wang, R.; Brooks, K. G.; Wu, J.; Dyakonov, V.; Yang, G.; Dai, S.; Dyson, P. J.; Nazeeruddin, M. K. Single-Crystalline TiO2 Nanoparticles for Stable and Efficient Perovskite Modules. *Nat. Nanotechnol.* **2022**, *17* (6), 598–605.

(8) Kim, M.; Jeong, J.; Lu, H.; Lee, T. K.; Eickemeyer, F. T.; Liu, Y.; Choi, I. W.; Choi, S. J.; Jo, Y.; Kim, H. B.; Mo, S. I.; Kim, Y. K.; Lee, H.; An, N. G.; Cho, S.; Tress, W. R.; Zakeeruddin, S. M.; Hagfeldt, A.; Kim, J. Y.; Grätzel, M.; Kim, D. S. Conformal Quantum Dot-SnO2 Layers as Electron Transporters for Efficient Perovskite Solar Cells. *Science.* **2022**, *375* (6578), 302–306.

(9) Gao, Y.; Liu, C.; Xie, Y.; Guo, R.; Zhong, X.; Ju, H.; Qin, L.; Jia, P.; Wu, S.; Schropp, R. E. I.; Mai, Y. Can Nanosecond Laser Achieve High-Performance Perovskite Solar Modules with Aperture Area Efficiency Over 21%? *Adv. Energy Mater.* **2022**, 2202287.

(10) Dai, X.; Chen, S.; Jiao, H.; Zhao, L.; Wang, K.; Ni, Z.; Yu, Z.; Chen, B.; Gao, Y.; Huang, J. Efficient Monolithic All-Perovskite Tandem Solar Modules with Small Cell-to-Module Derate. *Nat. Energy* **2022**, *7* (10), 923–931.

(11) Tang, M.; He, B.; Dou, D.; Liu, Y.; Duan, J.; Zhao, Y.; Chen, H.; Tang, Q. Toward Efficient and Air-Stable Carbon-Based All-Inorganic Perovskite Solar Cells through Substituting CsPbBr3 Films with Transition Metal Ions. *Chem. Eng. J.* **2019**, *375* (May), 121930.

(12) Wu, W.; Rudd, P. N.; Ni, Z.; Brackle, C. H. Van; Wei, H.; Wang, Q.; Ecker, B. R.; Gao, Y.; Huang, J. Reducing Surface Halide Deficiency for Efficient and Stable Iodide- Based Perovskite Solar Cells. *J. Am. Chem. Soc.* **2020**, *142* (8), 3989–3996.

(13) Jin, J.; Li, H.; Chen, C.; Zhang, B.; Xu, L.; Dong, B.; Song, H.; Dai, Q. Enhanced Performance of Perovskite Solar Cells with Zinc Chloride Additives. *ACS Appl. Mater. Interfaces* **2017**, *9* (49), 42875–42882.

(14) Uddin, M. A.; Glover, J. D.; Park, S. M.; Pham, J. T.; Graham, K. R. Growth of Highly Stable and Luminescent CsPbX3 (X = Cl, Br, and I) Nanoplates via Ligand Mediated Anion Exchange of CsPbCl3 Nanocubes with AlX3. *Chem. Mater.* **2020**, *32* (12), 5217–5225.

(15) Yu, Z.; Chen, X.; Harvey, S. P.; Ni, Z.; Chen, B.; Chen, S.; Yao, C.; Xiao, X.; Xu, S.; Yang, G.; Yan, Y.; Berry, J. J.; Beard, M. C.; Huang, J. Gradient Doping in Sn–Pb Perovskites by Barium Ions for Efficient Single-Junction and Tandem Solar Cells. *Adv. Mater.* **2022**, *34* (16), 2110351.

(16) Chen, B.; Rudd, P. N.; Yang, S.; Yuan, Y.; Huang, J. Imperfections and Their Passivation in Halide Perovskite Solar Cells. *Chem. Soc. Rev.* **2019**, *48* (14), 3842–3867.

(17) Chen, S.; Xiao, X.; Gu, H.; Huang, J. Iodine Reduction for Reproducible and High-Performance Perovskite Solar Cells and Modules. *Sci. Adv.* **2021**, *7* (10), eabe8130.

(18) Uddin, M. A.; Rana, P. J. S.; Ni, Z.; Dai, X.; Yu, Z.; Shi, Z.; Jiao, H.; Huang, J. Blading of

Conformal Electron-Transport Layers in p–i–n Perovskite Solar Cells. *Adv. Mater.* **2022**, *34* (30), 2202954.

(19) Zheng, X.; Chen, B.; Dai, J.; Fang, Y.; Bai, Y.; Lin, Y.; Wei, H.; Zeng, X. C.; Huang, J. Defect Passivation in Hybrid Perovskite Solar Cells Using Quaternary Ammonium Halide Anions and Cations. *Nat. Energy* **2017**, *2* (7), 17102.

(20) Uddin, M. A.; Hossain, T.; Kothalawala, N. L.; Joy, S.; Kim, D.-Y.; Graham, K. R. Multifunctional Thiol-Containing Additives for Improved Photoluminescence and Photovoltaic Performance of Cs0.15FA0.85PbI3 Perovskites. *ACS Appl. Electron. Mater.* **2022**, *4* (3), 903–909.

(21) Wang, R.; Xue, J.; Wang, K. L.; Wang, Z. K.; Luo, Y.; Fenning, D.; Xu, G.; Nuryyeva, S.; Huang, T.; Zhao, Y.; Yang, J. L.; Zhu, J.; Wang, M.; Tan, S.; Yavuz, I.; Houk, K. N.; Yang, Y. Constructive Molecular Configurations for Surface-Defect Passivation of Perovskite Photovoltaics. *Science.* **2019**, *366* (6472), 1509–1513.

(22) Cao, Q.; Li, Y.; Zhang, H.; Yang, J.; Han, J.; Xu, T.; Wang, S.; Wang, Z.; Gao, B.; Zhao, J.; Li, X.; Ma, X.; Zakeeruddin, S. M.; Sha, W. E. I.; Li, X.; Grätzel, M. Efficient and Stable Inverted Perovskite Solar Cells with Very High Fill Factors via Incorporation of Star-Shaped Polymer. *Sci. Adv.* **2021**, *7* (28), eabg0633.

(23) Uddin, M. A.; Mobley, J. K.; Masud, A. Al; Liu, T.; Calabro, R. L.; Kim, D.-Y.; Richards, C. I.; Graham, K. R. Mechanistic Exploration of Dodecanethiol Treated Colloidal CsPbBr3 Nanocrystals With Photoluminescence Quantum Yields Reaching Near 100%. *J. Phys. Chem. C* **2019**, *123* (29), 18103–18112.

(24) Wu, W. Q.; Rudd, P. N.; Wang, Q.; Yang, Z.; Huang, J. Blading Phase-Pure Formamidinium-Alloyed Perovskites for High-Efficiency Solar Cells with Low

Photovoltage Deficit and Improved Stability. *Adv. Mater.* **2020**, *32* (28), 2000995.

(25) Pan, S.; Wang, X.; Ni, C.; Hu, J. Nucleophilic Trifluoromethylation of Azinium Salts with Zn(CF3)2·bpy. *Tetrahedron* **2021**, *100*, 132477.

(26) Zhang, Y.; Peng, P.; Ying, Z.; Zhu, Q.; Zhou, J.; Wang, Z.; Liu, J.; Cen, K. Experimental Investigation on Multiphase Bunsen Reaction in the Thermochemical Sulfur-Iodine Cycle. *Ind. Eng. Chem. Res.* **2014**, *53* (8), 3021–3028.

(27) Ni, Z.; Xu, S.; Huang, J. Resolving Spatial and Energetic Distributions of Trap States in Metal Halide Perovskite Solar Cells. *Science.* **2021**, *371* (6532), 1352–1358.

(28) Ni, Z.; Jiao, H.; Fei, C.; Gu, H.; Xu, S.; Yu, Z.; Yang, G.; Deng, Y.; Jiang, Q.; Liu, Y.; Yan, Y.; Huang, J. Evolution of Defects during the Degradation of Metal Halide Perovskite Solar Cells under Reverse Bias and Illumination. *Nat. Energy* **2022**, *7* (1), 65–73.

(29) Baca, S. G.; Simonov, Y. A.; Gerbeleu, N. V.; Gdaniec, M.; Bourosh, P. N.; Timco, G. A. Synthesis and X-Ray Diffraction Study of Zn(II) Complexes with o-Phthalic Acid and Aromatic Amines. *Polyhedron* **2001**, *20* (9–10), 831–837.

(30) Chowdhury, T.; Dasgupta, S.; Khatua, S.; Acharya, K.; Das, D. Executing a Series of Zinc(II) Complexes of Homologous Schiff Base Ligands for a Comparative Analysis on Hydrolytic, Antioxidant, and Antibacterial Activities. *ACS Appl. Bio Mater.* **2020**, *3* (7), 4348–4357.

(31) Yamaguchi, T.; Lindqvist, O.; Trysberg, L.; Uggla, R.; Nielsen, P. H. The Crystal Structure of Tetraamminezinc(II) Diiodide, Zn(NH3)4I2. *Acta Chemica Scandinavica*. 1981, pp 811–814.

## Supplementary Files

This is a list of supplementary files associated with this preprint. Click to download.

- 20230402SupportingInformation.pdf